Journal of Hydrology 531 (2015) 111–123

Contents lists available at ScienceDirect

Journal of Hydrology

journal homepage: www.elsevier.com/locate/jhydrol

Characterisation of river–aquifer exchange fluxes: The role of spatial patterns of riverbed hydraulic conductivities

Q. Tang [a,b,*], W. Kurtz [a,b], P. Brunner [c], H. Vereecken [a,b], H.-J. Hendricks Franssen [a,b]

[a] Forschungszentrum Jülich GmbH, Institute for Bio- and Geosciences: Agrosphere (IBG-3), 52425 Jülich, Germany
[b] Centre for High-Performance Scientific Computing in Terrestrial Systems, HPSC TerrSys, Geoverbund ABC/J, Jülich, Germany
[c] University of Neuchâtel, Centre for Hydrogeology and Geothermics, 2000 Neuchâtel, Switzerland

ARTICLE INFO

Article history:
Available online 17 August 2015

Keywords:
Data assimilation
Ensemble Kalman Filter
Riverbed characterisation
River–aquifer interaction
Non-MultiGaussian
Patterns
Normal score transformation

SUMMARY

Interactions between surface water and groundwater play an essential role in hydrology, hydrogeology, ecology, and water resources management. A proper characterisation of riverbed structures might be important for estimating river–aquifer exchange fluxes. The ensemble Kalman filter (EnKF) is commonly used in subsurface flow and transport modelling for estimating states and parameters. However, EnKF only performs optimally for MultiGaussian distributed parameter fields, but the spatial distribution of streambed hydraulic conductivities often shows non-MultiGaussian patterns, which are related to flow velocity dependent sedimentation and erosion processes. In this synthetic study, we assumed a riverbed with non-MultiGaussian channel-distributed hydraulic parameters as a virtual reference. The synthetic study was carried out for a 3-D river–aquifer model with a river in hydraulic connection to a homogeneous aquifer. Next, in a series of data assimilation experiments three different groups of scenarios were studied. In the first and second group of scenarios, stochastic realisations of non-MultiGaussian distributed riverbeds were inversely conditioned to state information, using EnKF and the normal score ensemble Kalman filter (NS-EnKF). The riverbed hydraulic conductivity was oriented in the form of channels (first group of scenarios) or, with the same bimodal histogram, without channelling (second group of scenarios). In the third group of scenarios, the stochastic realisations of riverbeds have MultiGaussian distributed hydraulic parameters and are conditioned to state information with EnKF. It was found that the best results were achieved for channel-distributed non-MultiGaussian stochastic realisations and with parameter updating. However, differences between the simulations were small and non-MultiGaussian riverbed properties seem to be of less importance for subsurface flow than non-MultiGaussian aquifer properties. In addition, it was concluded that both EnKF and NS-EnKF improve the characterisation of non-MultiGaussian riverbed properties, hydraulic heads and exchange fluxes by piezometric head assimilation, and only NS-EnKF could preserve the initial distribution of riverbed hydraulic conductivities.

1. Introduction

Exchange processes between surface water and groundwater play an essential role for hydrology, hydrogeology, ecology, and water resources management (Brunke and Gonser, 1997; Hayashi and Rosenberry, 2002; Sophocleous, 2002). The main uncertain factors for predicting river–aquifer water exchange fluxes are riverbed and aquifer properties (Saenger et al., 2005; Storey et al., 2003). A better characterisation of riverbed structures representing more realistic properties may lead to an improved estimation of river–aquifer exchange fluxes (Kurtz et al., 2012). Traditionally, these media are considered homogeneous (Fox and Durnford, 2003) and the models for quantifying the exchange fluxes are simplified.

Field measurements and inverse modelling show that in the real world riverbed hydraulic conductivities may vary over several orders of magnitude (Calver, 2001). Several field surveys also indicate that the spatial distribution of river bed hydraulic conductivities exhibit non-Gaussian features (e.g., Cheng et al., 2011; Genereux et al., 2008; Leek et al., 2009; Sebok et al., 2015; Springer et al., 1999). Springer et al. (1999) found a bimodal distribution of hydraulic conductivity for five reattachment bars in the Colorado River (Grand Canyon National Park, USA). Genereux et al. (2008) conducted a detailed field experiment in a 250 m long river reach of West Bear Creek (North Carolina, USA) and found that measured river bed hydraulic conductivities are neither

* Corresponding author at: Forschungszentrum Jülich GmbH, Institute for Bio- and Geosciences: Agrosphere (IBG-3), 52425 Jülich, Germany.
E-mail address: q.tang@fz-juelich.de (Q. Tang).

http://dx.doi.org/10.1016/j.jhydrol.2015.08.019
0022-1694/

normally nor log-normally distributed. Cheng et al. (2011) measured vertical streambed hydraulic conductivities at 18 sites along a 300 km reach of Platte River (Nebraska, USA) and evaluated whether the measured values were normally distributed. For nine sites a normal distribution could be confirmed by several statistical tests. However, for the other sites the statistical tests were not significant, which was attributed to the presence of river tributaries with varying sediment loads. Several studies also suggest that there can be a distinct spatial pattern of cross-sectional river bed hydraulic conductivities (e.g., Genereux et al., 2008; Min et al., 2013; Sebok et al., 2015), which is thought to be related to flow velocity dependent spatially distinct sedimentation and erosion patterns. Some papers (e.g., Genereux et al., 2008; Leek et al., 2009; Sebok et al., 2015) additionally provide maps of the spatial distribution of measured river bed conductivities showing spatial patterns that can hardly be described by a purely Gaussian distribution.

Flow and transport modelling indicates that heterogeneity of riverbed properties has a large impact on river–aquifer exchange fluxes (Irvine et al., 2012; Kalbus et al., 2009; McCallum et al., 2014; Salehin et al., 2004; Woessner, 2000; Wroblicky et al., 1998). In earlier work, we analysed temporal changes in river bed hydraulic conductivities, which could be generated by floods and sedimentation processes (Kurtz et al., 2012). It was found that sequential data assimilation can detect the changes in the river bed with some delay. Kurtz et al. (2014) analysed the value of temperature measurements to characterise heterogeneous riverbeds. In other works it was analysed whether heterogeneous riverbeds (with Gaussian distributed heterogeneous riverbed conductivities) can be replaced with a few zones with spatially homogeneous riverbed conductivities (Kurtz et al., 2013). In practice not enough detailed knowledge is available on the spatial variation of riverbed hydraulic conductivities and Gaussian statistics are used for modelling, if heterogeneity is taken into account at all. However, non-Gaussian patterns probably have a significant influence on the magnitude and the spatial patterns of river–aquifer exchange fluxes, which can be of great importance for the prediction of transport processes of heat and contaminants in river–aquifer systems. Non-MultiGaussian patterns of riverbed hydraulic conductivities could result in very different net exchange fluxes between streams and aquifers compared to MultiGaussian distributions with the same geostatistical parameters. It was demonstrated that non-MultiGaussian patterns in aquifers result in a flow and transport behaviour which is very different from MultiGaussian patterns with the same global statistics (e.g., Gómez-Hernández and Wen, 1998; Zinn and Harvey, 2003). Fleckenstein et al. (2006) and Frei et al. (2009) represented facies distribution of aquifer heterogeneities and investigated the dynamics of river–aquifer exchange fluxes. However, in their studies, only aquifer heterogeneities were treated as non-MultiGaussian and riverbed hydraulic conductivities were the same as the underlying aquifer hydraulic conductivities. Consequently, until now, such non-MultiGaussian patterns have not been taken into account for the generation of riverbed hydraulic conductivities; neither were non-MultiGaussian distributed conductivities updated using inverse methods or data assimilation. This study therefore focuses on investigating the impact of the non-MultiGaussian distribution of riverbed hydraulic conductivities on model states and river–aquifer exchange fluxes.

A number of already established simulation techniques developed to characterise the spatial variability of aquifer heterogeneities (Khodabakhshi and Jafarpour, 2013; Zinn and Harvey, 2003) can also be applied for the characterisation of spatially variable riverbed structures. Geostatistical simulation techniques can model spatial heterogeneity by generating equally likely stochastic realisations of the spatially variable geological medium. One typical approach is the sequential simulation algorithm (Gómez-Hernández and Journel, 1993) based on a variogram to generate a conditional realisation from a MultiGaussian random function. Elfeki and Dekking (2001) proposed a Markov chain model to characterise geological heterogeneities constrained on well data. Another approach is the multiple-point (MP) geostatistical technique (Guardiano and Srivastava, 1993) which expanded the traditional sequential simulation by avoiding the definition of a random function based on two-points geostatistics (Hu and Chugunova, 2008). A comparison between simulations generated by the multiple-point geostatistical method and variogram-based geostatistics showed that the reproduction of the hydraulic conductivity field generated by MP methods can better represent certain geological media (Mariethoz et al., 2010). We assume that the multiple-point geostatistical method can also be used to generate more realistic parameter distributions of riverbeds. A next step is the inverse conditioning of the non-MultiGaussian parameter distribution to hydraulic head data.

Inverse modelling techniques are also called indirect methods which encompass model identification and parameter estimation. Carrera et al. (2005) reviewed the recent progress of inverse modelling for aquifer characterisation and tried to find similarities between well-established methods, including the pilot point method, zonation method and sequential self-calibration. Carrera and Neuman (1986) used a maximum likelihood method called the zonation method to estimate hydraulic conductivities and possibly other parameters for a limited number of zones in which the aquifer is divided. The division of the aquifer in a limited number of zones reduces the number of parameters to be estimated and allows a unique, stable solution of the inverse problem. Carrera and Neuman (1986) proposed the solution of the inverse problem by an iterative approach solving the groundwater flow problem, which results in a hydraulic head solution which is consistent with the parameters. RamaRao et al. (1995) proposed the pilot point method for solving the inverse problem in groundwater flow systems, locating pilot points where there are no measurements. The sequential self-calibration method was proposed by Gómez-Hernánez et al. (1997) and generates equally likely realisations of transmissivity fields conditioned to both transmissivities and heads. The main step forward of this approach is that a non-unique solution is sought to the inverse problem and multiple equally likely solutions are calculated. A comparison of seven inverse modelling methods for groundwater flow was presented by Hendricks Franssen et al. (2009). They showed that Monte Carlo based inverse modelling methods, which calculate multiple equally solutions to the inverse problem, generally outperform other inverse methods.

The Ensemble Kalman Filter (EnKF) (Evensen, 1994) is a Monte Carlo based inverse method. Instead of calculating one solution with a dynamical simulation model (in this paper a hydrological model) multiple solutions are calculated. The multiple solutions are calculated for different model inputs, like for example different spatial distributions of input parameters. Also other model input can be made uncertain. The different model inputs characterise the model input uncertainties and are sampled from multivariate probability density functions. The multiple solutions are used to calculate the model covariance matrix, containing the covariances between all model states. EnKF is a purely stochastic method because the observations are treated as random variables by adding perturbations to the measurements (Burgers et al., 1998). EnKF can be extended to estimate parameters together with states and was applied for estimating hydraulic conductivities for a transient groundwater flow problem by Chen and Zhang (2006). As it is suited to condition to observations and performs well for non-linear models, it becomes a robust tool to deal with flow and transport problems in complex geological media. Hendricks Franssen and

Kinzelbach (2008) used EnKF combined with the 2-D saturated transient groundwater flow equation to update both model states and parameters. A damping factor was introduced to avoid the filter inbreeding problem, which is an underestimation of the model variance related to a limited number of ensemble members used to approximate the model covariance matrix. Camporese et al. (2009) estimated stream flow using the CATHY model and incorporated the assimilation of both stream flow and pressure head data for two synthetic cases: a soil column experiment and a V-catchment scale experiment. Results showed that EnKF increased the accuracy of the prediction. Also Bailey and Baù (2010, 2012), and Pasetto et al. (2012), amongst others, analysed joint assimilation of pressure and discharge data for a coupled surface–subsurface problem. These papers however did not focus specifically on the riverbed and did not update riverbed hydraulic properties. Hendricks Franssen et al. (2011) jointly updated aquifer hydraulic conductivities and leakage coefficients in a real-time application of EnKF for the Limmat Valley aquifer in Zurich, Switzerland. Kurtz et al. (2012) characterised time-dependent leakage coefficients by updating time-dependent model parameters with EnKF using covariance inflation to improve the estimation performance. Kurtz et al. (2013) updated spatially variable leakage coefficients.

EnKF only works optimally when parameters or states follow a Gaussian distribution. Kerrou et al. (2008) investigated and compared the ability of direct methods and inverse modelling in characterising non-MultiGaussian parameter fields under the wrong assumption of a MultiGaussian random function model. They observed that two points MultiGaussian techniques were not able to detect the non-MultiGaussian structures and may lead to inaccurate groundwater flow and mass transport predictions. However, it is unclear whether river–aquifer exchange fluxes are affected in a similar way to flow and transport in aquifers. One approach to deal with non-Gaussian patterns of states and parameters is provided by Sun et al. (2009). They combine a grid-based EnKF with a Gaussian mixture modelling approach for handling non-Gaussian distributions. Another solution is the implementation of a normal score transformation which renders states and parameters Gaussian (Zhou et al., 2011) using anamorphosis functions for log-conductivities and piezometer heads. Zhou et al. (2011) showed that the Normal Score Ensemble Kalman Filter (NS-EnKF) outperforms the standard EnKF both in terms of characterising hydraulic conductivities and updating piezometer heads, and in a later work (Zhou et al., 2012) it was found that superior results are achieved even when no hydraulic conductivity data are available. Li et al. (2012) showed that NS-EnKF still outperforms EnKF in case of a wrong assumption about the prior geostatistical model, but a reasonable estimate of the histogram of the conductivity data is needed for the model to be successful. Schöniger et al. (2012) indicated that for variables showing complex dependency structures in space like solute concentration, NS-EnKF might not outperform classical EnKF. Crestani et al. (2013) corroborated these results and found that a modified NS-EnKF, with one normal score transformation for all grid nodes (not grid node specific) gave better results than the original NS-EnKF.

In this work, as a synthetic reality a non-MultiGaussian distribution of riverbed hydraulic conductivities is assumed. Note that previous studies considered riverbed heterogeneities as Gaussian distributed patterns. However, as motivated before, in the real world non-Gaussian riverbed properties are expected to be common. Given this non-Gaussian distribution, we want to analyse the impact of the adopted geostatistical model (either the MultiGaussian one or a non-MultiGaussian distribution) on the identification of model states, parameters and fluxes that characterise the river–aquifer interaction. How significant are the inaccuracies introduced if we impose a MultiGaussian distribution of riverbed properties when in reality properties are non-MultiGaussian? This work aims at analysing how well data assimilation methods like the EnKF or the NS-EnKF can inversely condition these riverbed conductivities, and whether the NS-EnKF outperforms the more classical EnKF for non-MultiGaussian distributions. The non-MultiGaussian fields of riverbed hydraulic conductivities are modelled with multiple-point geostatistical methods. In summary, this paper investigates: (i) how important it is to represent non-MultiGaussian distributions of riverbed hydraulic conductivities in the model (comparison with MultiGaussian assumption and an alternative erroneous non-MultiGaussian assumption), and (ii) whether NS-EnKF can outperform classical EnKF for the characterisation of non-MultiGaussian riverbeds under the non-MultiGaussian assumption. For the first objective, experiments with three different geostatistical models for riverbed characterisation were made: a non-MultiGaussian model exhibiting channels, a non-MultiGaussian model with the same bimodal histogram but without channels and a MultiGaussian model with the same mean and variance as the non-MultiGaussian models. Next, EnKF experiments were performed for the three geostatistical models by assimilating hydraulic heads with update of both states and parameters. Additionally, NS-EnKF was implemented for the two non-MultiGaussian models to evaluate the performance of normal score transformation. A series of numerical experiments are carried out with a three-dimensional synthetic river–aquifer model for different scenarios. The performance of EnKF/NS-EnKF is evaluated in terms of its ability to predict the hydraulic heads, reproduce the riverbed hydraulic conductivity fields and estimate the exchange fluxes between river and aquifer.

2. Methods and materials

2.1. Flow equations

The governing continuity hydraulic equation for a 3D unsaturated–saturated groundwater flow problem in a river–aquifer system is given by (Bear, 1979):

$$\frac{\partial}{\partial t}(\rho_w n S_w) = \nabla \cdot \left[\frac{\rho_w k k_{rw}(S_w)}{\mu_w}(\nabla p_w + \rho_w g \nabla z)\right] + q$$

where t is time (T), ρ_w is density of water (M L^{-3}), n is porosity, S_w is saturation, k is permeability (L^2), k_{rw} is relative permeability, μ_w is dynamic viscosity (M L^{-1} T^{-1}), p_w is pressure (M L^{-1} T^{-2}), g is gravitational acceleration (L T^{-2}), z is the elevation above sea (L), q are sources and sinks (M L^{-3} T^{-1}).

The software SPRING (Delta h Ingenieugesellschaft mbH, 2006) is used to solve the 3D unsaturated–saturated groundwater flow problem in a river–aquifer system with help of the finite element method, using regular rectangles in the simulation studies presented in this paper.

Boundary conditions used to solve this equation include fixed pressure (potential) heads and river stages. The river stages influence the vertical exchange fluxes Q between river and aquifer (L^3 T^{-1}). Q is considered as a third type boundary condition for solving the flow equation and is implemented in SPRING by

$$Q = \alpha A(h_{river} - h_{gw})$$

where α is leakage coefficient (T^{-1}), A is the area of the river bed where exchange fluxes occur (L^2), h_{river} is the river stage (L), and h_{gw} is the groundwater level (L). For unsaturated flow, relationships between pressure heads and saturation and k_{rw} were based on Van Genuchten equations (van Genuchten, 1980).

2.2. Normal score Ensemble Kalman Filter

The basic equations of EnKF and their application for identifying river bed conductivities are provided and discussed by Kurtz et al. (2012). Zhou et al. (2011) suggested the NS-EnKF scheme for updating states and parameters (piezometric heads and log-hydraulic conductivities). Here, we present the NS-EnKF in terms of the joint updating of piezometric heads and riverbed hydraulic conductivities (expressed as leakage coefficients (α)) with help of assimilation of piezometric heads to simulate river–aquifer interactions. The main steps and equations for NS-EnKF are summarised as follows:

1. Generation of initial ensemble. In our work, non-MultiGaussian distributed parameter fields are generated using the direct sampling algorithm (Mariethoz et al., 2010), a multiple-point geostatistical simulation technique (Caers and Zhang, 2004; Zhang, 2008). Both non-MultiGaussian fields with channels and non-MultiGaussian fields without channels are generated by the direct sampling algorithm. MultiGaussian distributed parameter fields are generated using a sequential MultiGaussian simulation technique (Gómez-Hernández and Journel, 1993).
2. Forecast of state vectors. In this step, the states at the current time step are estimated from the previous time step by the transient flow model. The stochastic realisations of $\log_{10}(\alpha)$, together with other input information, are used here as input to solve the 3-D river–aquifer flow problem with the software SPRING. The calculated piezometric heads are denominated "forecasted heads" in order to distinguish them from the updated heads after data assimilation. For each of the realisations, the prediction equation is given by:

$$\mathbf{h_{t,i}} = M(\mathbf{h_{t-1,i}}, \mathbf{p_{t-1,i}}, \mathbf{q_{t-1,i}})$$

where $\mathbf{h}$ is the state vector (here the simulated piezometric heads), $\mathbf{p}$ are the model parameters, $\mathbf{q}$ is the vector with model forcings, M is the simulation model (the river–aquifer model in this work, see Section 2.1), t is the time step counter and i is the realisation number. The length of the $\mathbf{h}$ vector is equal to the number of model nodes.
3. Normal-Score transformation. This is only done for certain simulation scenarios (see Section 3.4). The ensemble of state vector forecasts and leakage coefficient fields provides the basis for the normal-score transform of heads and leakage coefficients. At each location and time step a probability density function of hydraulic heads and leakage coefficients can be constructed. In addition, both simulated piezometric heads and leakage coefficients are transformed by creating anamorphosis functions for each variable independently, at all grid cell locations and all time steps. The anamorphosis function we use here is an estimator from Johnson and Wichern (2002):

$$y = G^{-1}[F(\mathbf{x})]$$

$$F_j = \frac{j - 0.5}{N}$$

where $\mathbf{x}$ is the original vector, F is the empirical cumulative distribution function (CDF), G is theoretical standard normal CDF, j is the rank of $\mathbf{x}$ and N is the sample size. Therefore, the transformed piezometric heads and transformed $\log_{10}(\alpha)$ can be written as:

$$\mathbf{h_{t,i}^{trans}} = G^{-1}\left[\frac{j_{h_{t,i}} - 0.5}{N}\right]$$

$$\log_{10}(\boldsymbol{\alpha}_{\mathbf{t,i}}^{\mathbf{trans}}) = G^{-1}\left[\frac{j_{\log_{10}(\alpha_{t,i})} - 0.5}{N}\right]$$

where α is leakage coefficient and the superscript *trans* indicates the variable after transformation.
4. Updating. In this step simulated heads, possibly transformed, from the model are compared with measurements, which are also transformed in case the simulated heads are transformed. The measurement equation given below shows how the measurements at observation locations are related to the, possibly transformed, simulated heads vector:

$$\mathbf{z_{t,i}} = \mathbf{H}\mathbf{h_{t,i}^{trans}}$$

where $\mathbf{H}$ is the measurement operator with dimension of $N_{obs.} \times N_{nodes.}$ consisting of 0 and 1, as it is assumed that the observations are exactly located at the grid nodes. The original measurements are perturbed with a series of normally distributed measurement errors. These measurement errors are defined a priori on the basis of expert knowledge:

$$\mathbf{y_{t,i}} = \mathbf{y_t} + \boldsymbol{\varepsilon}_{\mathbf{t,i}}$$

where $\mathbf{y_{t,i}}$ is the perturbed measurement vector, $\mathbf{y_t}$ is the vector with the measurements at the current time step and $\boldsymbol{\varepsilon}_{\mathbf{t,i}}$ is the vector containing random errors. If the perturbed measurements are transformed, this is done using the same anamorphosis function as for the simulated heads at that location. It is necessary to interpolate transformed heads or leakage coefficients along the anamorphosis function, since most measurements will not correspond exactly with one of the points that define the anamorphosis function and some may be outside the range. The linear spline is selected here for interpolation, as it has been proven to be a stable and reasonable choice when the ensemble size is large enough ($N > 200$) (Schöniger et al., 2012). The mean slope of the anamorphosis function was estimated and used for extrapolation, which was found to be a stable solution. The transformed perturbed measurements can be written as:

$$\mathbf{y_{t,i}^{trans}} = \phi(\mathbf{y_{t,i}})$$

where $\phi(\cdot)$ is the anamorphosis function created based on the simulated heads and the interpolation/extrapolation. Next, the Kalman gain $\mathbf{K}$ is calculated as:

$$\mathbf{K} = \mathbf{C}\mathbf{H}^{\mathbf{T}}(\mathbf{H}\mathbf{C}\mathbf{H}^{\mathbf{T}} + \mathbf{R})^{-1}$$

where $\mathbf{C}$ is the covariance matrix of the, possibly transformed, states and parameters and $\mathbf{R}$ is the covariance matrix of, possibly transformed, measurement errors. The structure of $\mathbf{C}$ for the example of transformed states and variables is as follows:

$$\mathbf{C} = \begin{pmatrix} \mathbf{C}_{\mathbf{h}^{\mathbf{trans}}\mathbf{h}^{\mathbf{trans}}} & \mathbf{C}_{\mathbf{h}^{\mathbf{trans}},\log\boldsymbol{\alpha}^{\mathbf{trans}}} \\ \mathbf{C}_{\log\boldsymbol{\alpha}^{\mathbf{trans}},\mathbf{h}^{\mathbf{trans}}} & \mathbf{C}_{\log\boldsymbol{\alpha}^{\mathbf{trans}}\log\boldsymbol{\alpha}^{\mathbf{trans}}} \end{pmatrix}$$

The analysis equation updates the transformed, simulated heads (and transformed $\log_{10}(\alpha)$) accounting for the observations:

$$\mathbf{X_{t,i}^{ana}} = \mathbf{X_{t,i}^{sim}} + a\mathbf{K}\left(\mathbf{y_{t,i}^{trans}} - \mathbf{H}\mathbf{h_{t,i}^{trans}}\right)$$

where $\mathbf{X_{t,i}^{ana}}$ is the updated augmented state vector, $\mathbf{X_{t,i}^{sim}}$ is the simulated vector, and a is the damping factor which acts only on the parameter updates, with a value between 0 and 1. The vector $\mathbf{X}$ contains also the transformed variables and parameters:

$$\mathbf{X} = \begin{pmatrix} \mathbf{h}^{\mathbf{trans}} \\ (\log_{10}(\boldsymbol{\alpha}))^{\mathbf{trans}} \end{pmatrix}$$

It should be noticed that it is also possible to transform only the heads or only $\log_{10}(\alpha)$ or none of the two. In the latter case the updating equation reduces to the standard EnKF-method for joint updating of states and parameters.

5. Back transformation if transformation was done at step 3. The updated heads (and $\log_{10}(\alpha)$) are back transformed after data assimilation using the inverse anamorphosis functions. For this step, the original anamorphosis functions are used but now in general interpolation/extrapolation is needed. After finishing this step, the algorithm returns to step 2.

3. Synthetic experiments

3.1. Model setup

We carried out numerical experiments for a simplified synthetic three-dimensional river–aquifer model with a domain size of 500 m × 250 m × 10 m, see Fig. 1. The model is discretized into 125,000 grid cells at a spatial resolution of 10 m × 10 m × 0.1 m. For two reasons a high vertical model resolution was chosen. The first reason is the improved representation of vertical variations in saturation. The second reason is the improvement of numerical stability. The simulation period of one year is discretized into 365 time steps. A river is conceptualised into eight lines of river nodes (408 nodes totally), which are situated in the top layer of the domain and are in fact nodes which represent the riverbed–aquifer interface, connected to the river. The river nodes are situated in the middle of the simulation domain. We assume that the aquifer is homogeneous and only the river bed is spatially heterogeneous. The aquifer has a log-transformed hydraulic conductivity of $-3\log_{10}$ m/s. The initial river stage at the western boundary is 410 m and decreases to the eastern boundary with a slope of 0.01. The model forcing data for this synthetic model are transient river stages calibrated from real world discharge data of river Sihl which are taken from Kurtz et al. (2014). See Fig. 2 (left) for further details. Otherwise, both western and eastern boundaries are impermeable. Northern and southern boundaries are assigned prescribed heads with a yearly cycle whose values are given by a phase shifted sine function with an amplitude of 1 m (see Fig. 2 (right)). Along the northern and southern boundaries, time dependent fixed heads are spatially homogeneous. A model spin-up of 50 days, using average hydrologic conditions, is made for both the reference runs and all other ensemble runs so that model states and parameters are in dynamic equilibrium and the values for the initial states are meaningful. The final simulated heads from the spin-up period were used as initial heads for the forward model run. This model set-up results in infiltration of river water into the aquifer in the western part of the model domain during most of the simulation period, whereas the opposite occurs most of the time in the eastern part of the simulation domain. Partially saturated conditions below the riverbed prevail in the eastern part of the domain. At 30 observation points piezometric head is monitored (ten measurements directly below the riverbed, for the uppermost model layer and others north and south of the river, also for the uppermost model layer) and no observations are available for constraining parameters (K and α). See also Fig. 1 for the position of the measurement locations. Fig. 2 provides a summary of the model dynamics and boundary conditions for both the reference runs and data assimilation runs. The temporal pattern of river stage variation is the same for each river node, but the absolute values of the river stage vary across the river nodes. Hydraulic parameters according to van Genuchten were employed for characterising flow under unsaturated conditions, using three different parameter combinations as provided by the software SPRING (for further details of the parameter values see Kurtz et al., 2013).

3.2. Multiple reference runs

For the synthetic experiment in total ten different reference fields of riverbed hydraulic conductivities were defined. The performance of different prior geostatistical models (see Section 3.3) was evaluated for each of the ten reference fields. Ten reference fields were generated instead of one reference field because results can be quite influenced by the specific features generated in the reference field (e.g., Schöniger et al., 2012).

For the generation of the ten non-MultiGaussian reference fields with channels, a training image is generated by SGeMS (Remy et al., 2009), which reflects the channelised structures, see Fig. 3. The training image is composed of two different facies, and the fraction of highly permeable facies (in red) is set to 0.4. In the training image, the channels correspond to sand and the background represents low permeable materials like clay. The direct sampling method (Mariethoz et al., 2010) is used as a multiple-point geostatistical simulation technique to generate the patterns for the non-MultiGaussian references with channels. In order to complete the generation of the non-MultiGaussian reference fields, the two facies were independently populated with log transformed leakage coefficient values generated by sequential Gaussian simulation using the GCOSIM3D code (Gómez-Hernández and Journel, 1993). Table 1 gives the geostatistical parameters for generating the MultiGaussian patterns within each of the facies of the non-MultiGaussian models. A spherical variogram model was adopted in all cases. The mean $\log_{10}(\alpha)$ of the riverbed channels was three orders of magnitude larger than the little permeable parts of the riverbed.

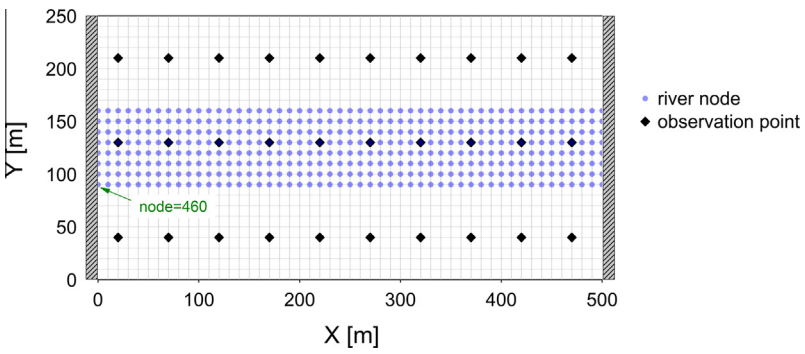

Fig. 1. Setup of the synthetic 3D model including the observation points and the nodes which are located below the river (in blue). Node number 460 is also indicated as a reference for Fig. 2. (For interpretation of the references to colour in this figure legend, the reader is referred to the web version of this article.)

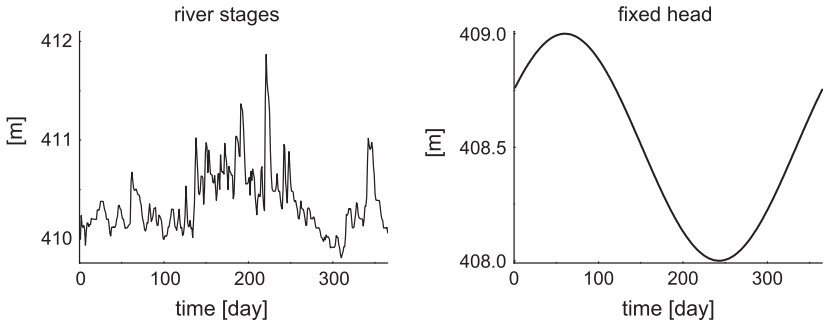

Fig. 2. Model dynamics and boundary conditions. (Left) temporal evolution of river stages at node = 460; (right) temporal evolution of fixed heads along northern and southern boundaries.

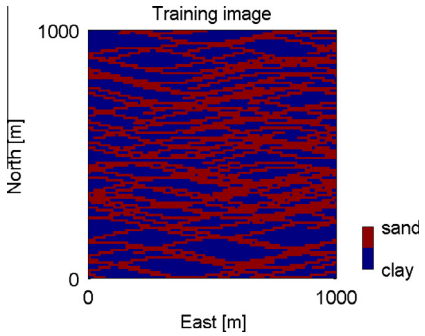

Fig. 3. The training image used for the generation of the ten non-MultiGaussian reference fields with channels.

The resulting reference $\log_{10}(\alpha)$ fields are shown in Fig. 4. Each reference field shows a pronounced bimodality with distributed connected channels (one example of the histograms for these reference fields is given in Fig. 5). Forward model runs are made for the ten reference fields for a simulation period of 365 days and the calculated heads serve to collect synthetic hydraulic head observations at 30 observation points. These synthetic data are assimilated on a daily basis in the data assimilation experiments. Piezometric head measurements are unbiased with a standard deviation of 0.05 m. No (riverbed) hydraulic conductivity data are available as direct data in the experiments.

3.3. Three geostatistical models for generation of riverbed heterogeneities

Three different a priori geostatistical models (used in data assimilation with EnKF) were used to investigate the role of patterns of riverbed heterogeneities:

Table 1
Variogram parameters used to generate stochastic realisations of $\log_{10}(\alpha)$ for each of the two facies in the non-MultiGaussian reference fields with channels. Background represents the material between the highly permeable channels/ellipsoidal structures. The same parameters were used to generate stochastic realisations for the non-MultiGaussian model with channels and the non-MultiGaussian model with ellipsoidal structures. The geostatistical parameters for creating stochastic realisations for the MultiGaussian model are also given.

Facies	Variogram type	Mean ($\log_{10}$(m/s))	Range (m)[a]	Sill ($\log_{10}$(m/s))
Channel (ellipsoidal)	Spherical	−2.0	100	0.5
Background	Spherical	−5.0	100	0.5
MultiGaussian	Spherical	−3.8	100	2.7

[a] In all directions (x, y and z).

(i) Non-MultiGaussian distributed riverbed properties with connected channels (same geostatistical model as reference).
(ii) Non-MultiGaussian distributed riverbed properties with the same bimodal distribution of $\log_{10}(\alpha)$ as in (i), but with ellipsoidal instead of channelised structures.
(iii) MultiGaussian distributed riverbed properties.

Notice that the only difference between (i) and (ii) is the spatial organisation of the riverbed hydraulic conductivities, the main difference being the spatial continuity, which is much higher for the channelised structures than for the ellipsoidal structures.

Table 1 provides also the basic statistics used to generate the stochastic realisations for each of the geostatistical models. Fig. 5 shows the log-conductivity histograms for the three geostatistical models.

Stochastic realisations for the two non-MultiGaussian models are generated with help of two training images created by SGeMS (Remy et al., 2009). The training image for the non-MultiGaussian model with channels is the same as detailed in Section 3.2, and the training image for the non-MultiGaussian model with ellipsoidal structures is shown in Fig. 6. This last training image is composed of two different facies, again with a proportion of 0.4 for the highly permeable facies to make the two training images comparable for geostatistical simulation. The direct sampling method (Mariethoz et al., 2010) is also used to generate facies distributed patterns for the two non-MultiGaussian models.

Stochastic realisations for the two non-MultiGaussian models are completed by populating the two facies independently with log-transformed leakage coefficient values. These leakage values are generated by sequential Gaussian simulation using the GCOSIM3D code (Gómez-Hernández and Journel, 1993), see Fig. 6. Table 1 gives the geostatistical parameters for generating the MultiGaussian patterns within each of the facies of the non-MultiGaussian models.

The MultiGaussian stochastic realisations of $\log_{10}(\alpha)$ are generated using GCOSIM3D with the same arithmetic mean and variance as for the non-MultiGaussian models. Fig. 7 provides examples of generated stochastic realisations of riverbed hydraulic conductivity fields, which are later used as initial ensembles of $\log_{10}(\alpha)$. Table 1 gives the geostatistical parameters used for defining the MultiGaussian random model. The variance of the riverbed $\log_{10}(\alpha)$ for the MultiGaussian case was selected in order to get a variance which is similar to the overall variance of the non-MultiGaussian case.

3.4. Data assimilation experiments

Simulations were performed with 200 stochastic realisations of leakage coefficients for eight scenarios and for each of the ten

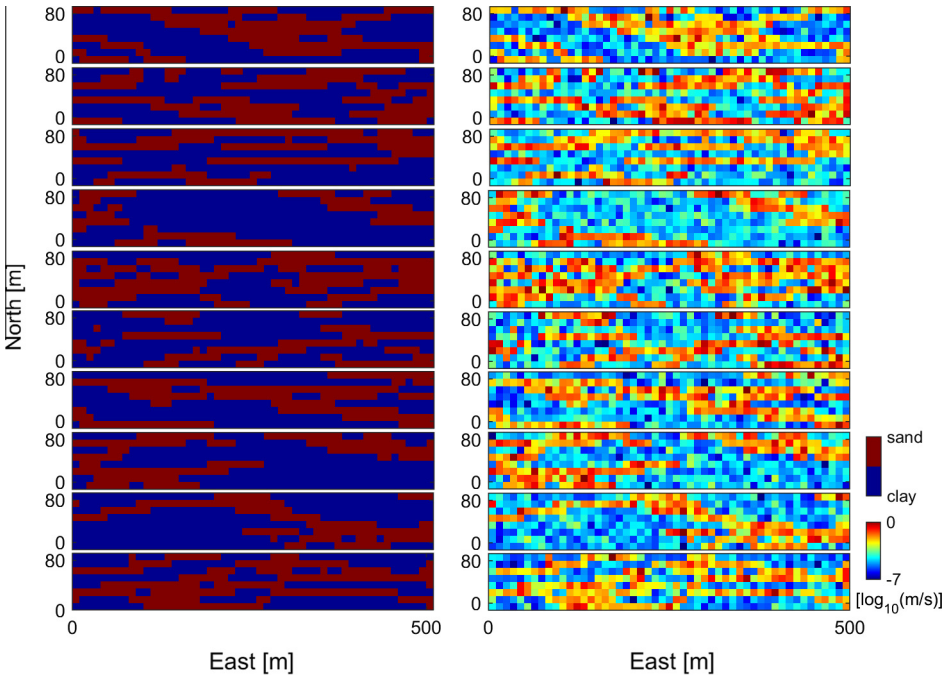

Fig. 4. (left) The ten reference facies distributions and (right) the ten associated reference distributions of $\log_{10}(\alpha)$.

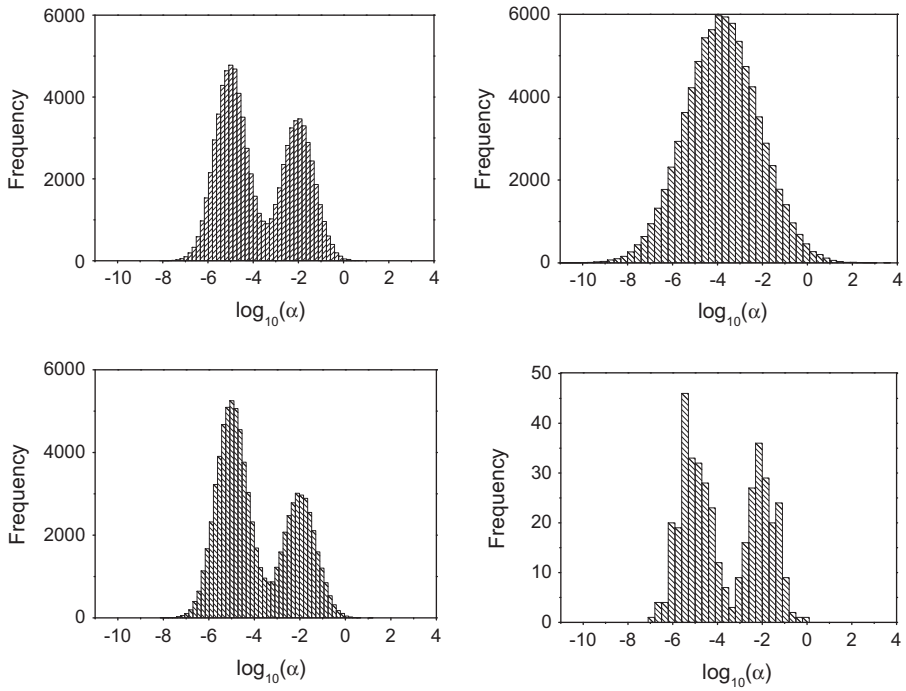

Fig. 5. Histograms of $\log_{10}(\alpha)$ calculated over all river nodes for the non-MultiGaussian model with channels (upper left), the MultiGaussian model (upper right), and the non-MultiGaussian model without channels (bottom left). The bottom right shows an example of a histogram for a true reference field (reference field number 1).

reference fields. The number of stochastic realisations was limited to 200 given restrictions on CPU-time. The stochastic realisations generated according to the three geostatistical models are the starting point for conditioning to hydraulic head data with help of data assimilation methods. Piezometric heads and leakage coefficients are updated with assimilation of piezometric heads. A damping factor a of 0.1 (Section 2.2) is used in the EnKF/NS-EnKF scheme. For comparison purpose, unconditional (open loop) simulations are performed with exactly the same model settings.

A detailed description of different scenarios is given in Table 2. As indicated before, three different geostatistical models were evaluated and for each of these models open loop simulations were performed (scenarios 1, 4 and 7). For each of the geostatistical models also joint updating of hydraulic heads and leakage coefficients with EnKF was evaluated (scenarios 2, 5 and 8). In addition, for the non-MultiGaussian models this updating was also evaluated with NS-EnKF (instead of EnKF), these are the scenarios 3 and 6.

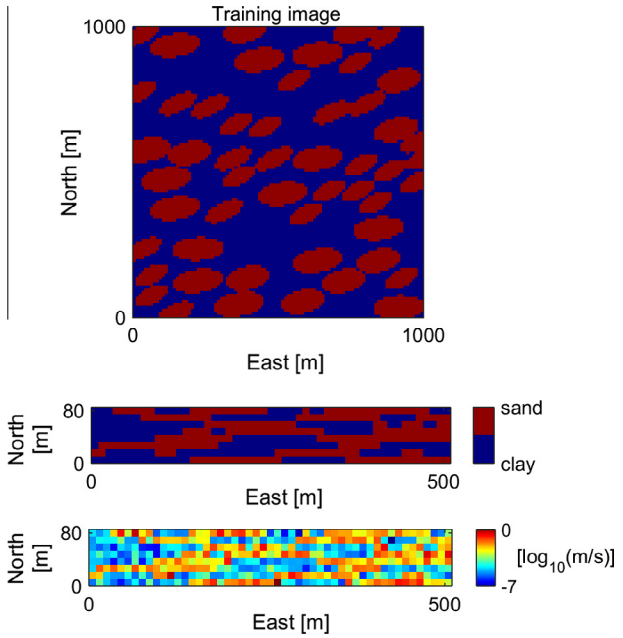

Fig. 6. Training images used to generate an ensemble of $\log_{10}(\alpha)$ realisations for non-MultiGaussian models with ellipsoidal structures (upper). The training image is squared and deviates from the rectangular riverbed as the training image serves as a database for geological structures, from which samples are taken. An example is provided of a stochastic realisation generated from the training image with channelised structures. First, a binary pattern of facies is generated with the direct sampling method (middle). Second, within each facies MultiGaussian distributed values are generated with GCOSIM3d (bottom).

3.5. Performance assessment

Performance evaluation measure is the root mean square error (*RMSE*) of model states (simulated heads), model parameters ($\log_{10}(\alpha)$) and leakage fluxes (Q) to quantify the difference between model predictions and reference values:

$$RMSE(X) = \sqrt{\frac{1}{N_r N_t N_{nodes}} \sum_{r=1}^{N_r} \sum_{t=1}^{N_t} \sum_{i=1}^{N_{nodes}} \left(X_{i,t,r}^{sim} - X_{i,t,r}^{ref} \right)^2}$$

where N_r is the number of realisations, N_t is the number of time steps, N_{nodes} is the total number of model nodes over the complete domain, the superscripts *sim* and *ref* refer to the model predictions at a certain time step before data assimilation and the reference values at the same time step, respectively. We calculated *RMSE* also for individual time steps:

$$RMSE(X,t) = \sqrt{\frac{1}{N_r N_{nodes}} \sum_{r=1}^{N_r} \sum_{i=1}^{N_{nodes}} \left(X_{i,t,r}^{sim} - X_{i,t,r}^{ref} \right)^2}$$

RMSE measures how close model predictions are to the true value over the complete model domain. We also calculated the relative error for evaluation, as it expresses the improvement compared to the open loop simulation.

$$R(X) = \frac{RMSE_{scenario}(X)}{RMSE_{openloop}(X)}$$

4. Results and discussion

The different scenarios described previously were analysed. The errors for simulated heads, updated $\log_{10}(\alpha)$ and estimated leakage fluxes calculated according to these different scenarios (Table 2) averaged over ten references are summarised in Table 3.

4.1. Influence of river bed patterns

This subsection centres on the impact of adopting a wrong geostatistical model for the spatial distribution of riverbed hydraulic conductivities and results are compared with the case that the correct model assumption was used. In particular, it is investigated whether the specific spatial pattern of $\log_{10}(\alpha)$ matters; non-MultiGaussian simulations with connected channels and disconnected ellipsoidal clusters are compared.

First, results are compared for a non-MultiGaussian model exhibiting channels, a non-MultiGaussian model with the same bimodal histogram but without channels and a MultiGaussian model. The comparison is centred here on the case hydraulic head data are used to update model states and $\log_{10}(\alpha)$, with EnKF (scenarios 2, 5 and 8 in Table 3). Errors for these three scenarios (in terms of *RMSE*) are smaller than for open loop simulations (scenario 1). For example, the relative improvement for *RMSE*(h) evaluated over all nodes was 27% and 29% for the MultiGaussian and the channelised scenarios, respectively and even 38% for the non-MultiGaussian ellipsoidal scenario. Updated $\log_{10}(\alpha)$ and leakage fluxes show less improvement, especially for the MultiGaussian assumption. The characterisation of $\log_{10}(\alpha)$ (results for leakage fluxes in brackets) in terms of *RMSE* improved 5% (9%) for MultiGaussian fields, 10% (18%) for non-MultiGaussian fields without channels and 9% (21%) for non-MultiGaussian with channels. In general, from Table 3 it can be observed that for non-MultiGaussian fields with channels the characterisation of leakage coefficients and fluxes improves more with data assimilation than for the other geostatistical models which used the wrong model assumption. However, the differences between the two non-MultiGaussian models are only small and probably not significant.

The temporal evolution of *RMSE* for simulated heads for different scenarios is shown in Fig. 8. At the beginning of the simulation period, we cannot observe a pronounced benefit from data assimilation. However, after 100 days EnKF improves the simulation results compared to the open loop run and the

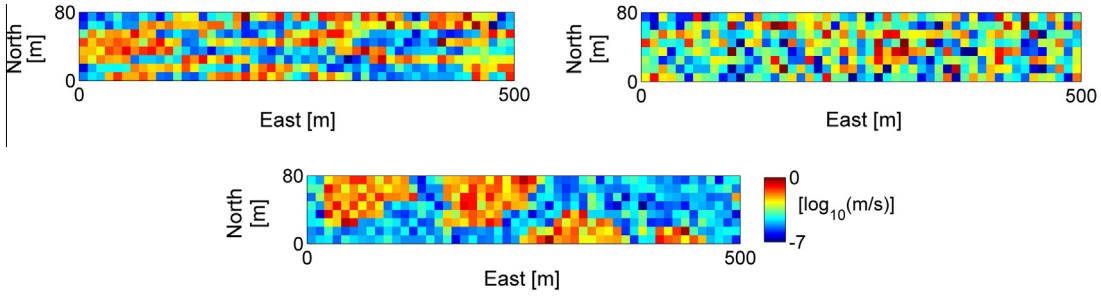

Fig. 7. Examples of stochastic realisations of $\log_{10}(\alpha)$ drawn from the non-MultiGaussian model with channels (upper left), the MultiGaussian model (upper right) and the non-MultiGaussian model without channels (bottom).

Table 2
Definition of the eight simulation scenarios (open loop and five different data assimilation scenarios).

Assumption	Scenarios	Update h	Update α	Transform h	Transform α
Non-MultiGaussian (channel)	1: open loop	×	×	×	×
	2: hl	√	√	×	×
	3: hl_hl	√	√	√	√
Non-MultiGaussian (ellipsoidal)	4: ellip_open loop	×	×	×	×
	5: ellip_hl	√	√	×	×
	6: ellip_hl_hl	√	√	√	√
MultiGaussian	7: multi_open loop	×	×	×	×
	8: multi_hl	√	√	×	×

√: yes. ×: no.

Table 3
Performance measures (standardised, relative errors) for the different scenarios averaged over ten references.

Simulation scenarios	$RMSE_{allnodes}(h)$	$RMSE$ (α)	$RMSE$ (Q)
1: open loop	1.00	1.00	1.00
2: hl	0.73	0.91	0.79
3: hl_hl	0.72	0.93	0.84
4: ellip_openloop	1.00	1.00	1.00
5: ellip_hl	0.62	0.90	0.82
6: ellip_hl_hl	0.60	0.92	0.85
7: multi_openloop	1.00	1.00	1.00
8: multi_hl	0.71	0.95	0.91

non-MultiGaussian model with channels performs better than the MultiGaussian model and the non-MultiGaussian model with ellipsoidal structures, for this specific reference. In general, data assimilation results in an improved characterisation of hydraulic heads compared to the open loop run, but the differences are not very large. To analyse the ability of characterisation of riverbed hydraulic conductivities, the temporal evolution of *RMSE* for updated $\log_{10}(\alpha)$ is shown in Fig. 9. Fig. 9 illustrates that a non-MultiGaussian model with channels outperforms the other geostatistical models.

Fig. 10 displays the final updated ensemble mean $\log_{10}(\alpha)$ fields for the scenarios 2, 5 and 8. After one year of assimilation, the updated $\log_{10}(\alpha)$ field for the case with channels captures the basic structures of the reference field, although the absolute magnitude for the leakage values differs from the reference. For the MultiGaussian case the updated riverbed patterns are similar to the initial distribution, and hardly recover the basic patterns of the reference field from the measurement data.

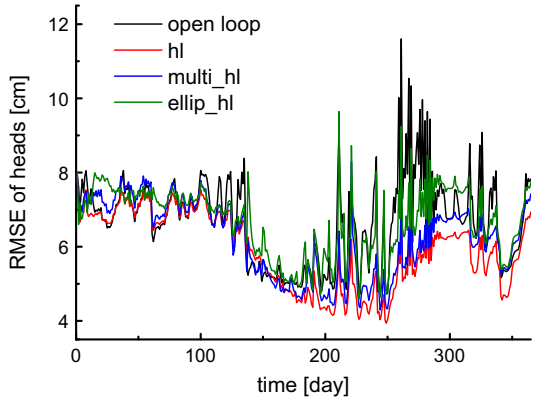

Fig. 8. Temporal evolution of RMSE for simulated heads evaluated over all model nodes and all realisations after each time step (for reference 1). Displayed are the RMSE for the open loop run and scenarios with different patterns for riverbed hydraulic conductivities, conditioned on hydraulic head data with EnKF.

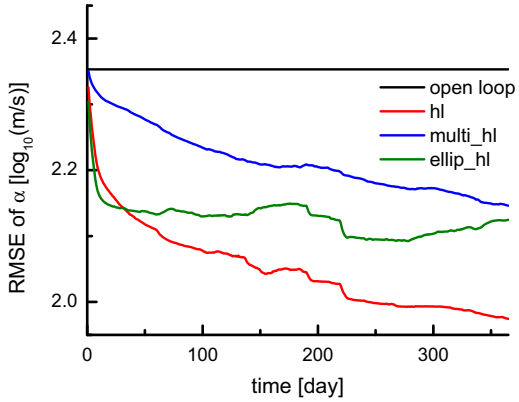

Fig. 9. Temporal evolution of RMSE of updated $\log_{10}(\alpha)$, evaluated over all river nodes and all realisations after each time step (for reference 1). Displayed are open loop run and scenarios with different riverbed hydraulic conductivity patterns, conditioned on hydraulic head data with EnKF.

Although EnKF improves the characterisation of riverbed hydraulic conductivity for the non-MultiGaussian conditions, none of them could preserve the bimodal histogram.

Fig. 11 shows the boxplot of *RMSE* of piezometric heads, updated $\log_{10}(\alpha)$ and leakage fluxes, calculated over ten reference fields and for different scenarios. Root mean square errors are lower after data assimilation (compared to open loop simulations).

The comparison of the performance of the three geostatistical models reveals that best results are obtained with a non-MultiGaussian model with channels and the non-MultiGaussian model with ellipsoidal structures. It is not surprising that the non-MultiGaussian model with channels performs best, as all ten reference fields were also drawn from this geostatistical model. Again, it is more remarkable that the other non-MultiGaussian model performs similar, pointing to the fact that the statistical distribution of leakage coefficients matters, but not so much the spatial pattern of it. If – erroneously – a MultiGaussian model is assumed for $\log_{10}(\alpha)$, results are worse, especially for characterisation of leakage coefficients and to a lesser extent also for flux characterisation. However, the characterisation of fluxes is not so much affected as typically is found in groundwater studies (e.g., Gómez-Hernández and Wen, 1998; Zinn and Harvey, 2003). For example, synthetic experiments on groundwater flow and transport of solutes in groundwater revealed that breakthrough of contaminants can be much faster in time when channels are present, compared to the MultiGaussian case (e.g., Wen and Gómez-Hernández, 1998). In addition, it was found that inverse modelling with an erroneous MultiGaussian assumption for a non-MultiGaussian aquifer is not able to delineate channels or improve transport predictions significantly, stressing the importance of the correct adoption of the geostatistical model for the aquifer (Kerrou et al., 2008). This might indicate that non-MultiGaussian riverbed patterns

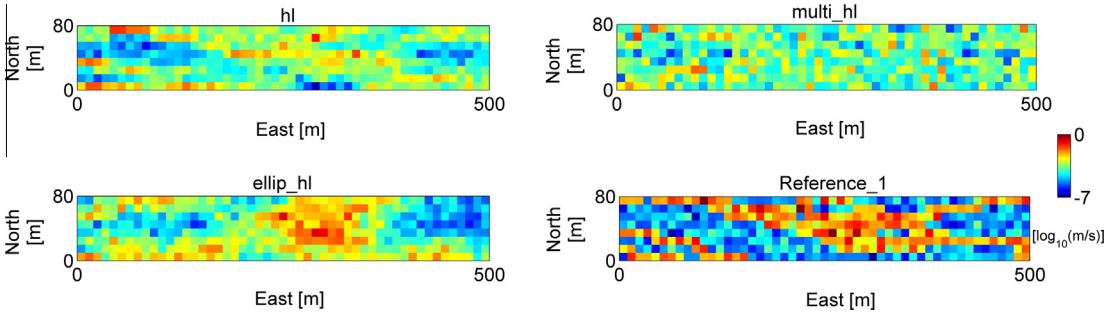

Fig. 10. The reference $\log_{10}(\alpha)$ field together with final updated $\log_{10}(\alpha)$ fields (ensemble mean) after 365 time steps with EnKF for the three simulation scenarios: (upper, left) hl: non-MultiGaussian model with channels; (upper, right) multi_hl: MultiGaussian model; (bottom, left) ellip_hl: non-MultiGaussian model without channels and (bottom, right): Reference field number 1.

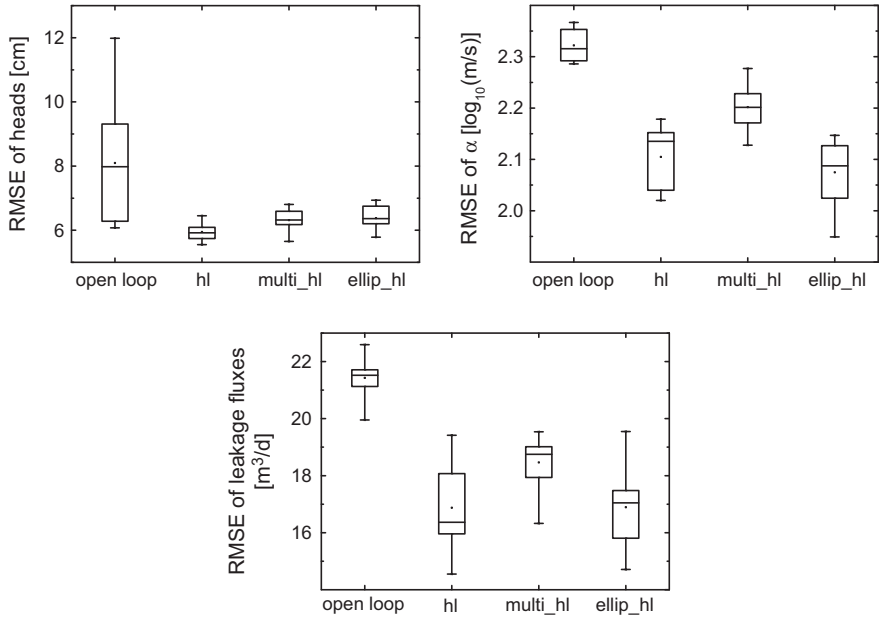

Fig. 11. Boxplot over ten references for (upper left) simulated heads, (upper right) updated $\log_{10}(\alpha)$ and (bottom) estimated leakage fluxes over all model (river) nodes, all realisations and all time steps for scenarios starting with different riverbed hydraulic conductivity patterns.

matter less for flow characterisation than non-MultiGaussian aquifer patterns. This is most probably related to the vertical water fluxes through the riverbed, so that horizontally oriented channels have less influence on the flow, whereas in aquifers flow is predominantly horizontal and controlled by channels.

It was assumed in this study that geostatistical parameters which describe spatial heterogeneity of riverbed hydraulic conductivities within the facies are perfectly known. In reality these parameters are (very) uncertain as well. It is expected that this assumption has not a major impact on the outcomes of this study. For the case that a MultiGaussian assumption was adopted, assuming correlation structures which deviate strongly from the non-MultiGaussian reference, the performance was not much worse than for the case with the correct, non-MultiGaussian assumption. It is expected that a minor mistake in the correlation structure within facies would have a smaller impact. For the same reasons, it is expected that a mistake in the training image would also have a more limited impact in this study. Uncertainty of the training image was not studied in this paper, but first studies have been published where uncertainty of the training image was considered (e.g., Khodabakhshi and Jafarpour, 2013).

4.2. Performance of NS-EnKF (EnKF versus NS-EnKF)

Results presented in Section 4.1 were generated by data assimilation using the classical Ensemble Kalman Filter. EnKF is suboptimal for non-MultiGaussian distributions and therefore NS-EnKF was tested as an alternative data assimilation procedure. The results obtained with EnKF (Section 4.1) showed that the bimodal distribution of $\log_{10}(\alpha)$ could not be captured even although some of the simulations with EnKF started from a bimodal distribution.

Normal score transformation of both hydraulic heads and $\log_{10}(\alpha)$ was done in the simulation scenarios 3 and 6, which will be compared with the simulation scenarios 2 and 5. For hydraulic head characterisation, it is indeed found that NS-EnKF gives better results than classical EnKF, with a 1–2% additional reduction of *RMSE* (see Table 3). However, the characterisation of leakage coefficients and leakage fluxes slightly worsens with NS-EnKF (compared to classical EnKF).

Figs. 12 and 13 show the histograms and updated leakage coefficient fields, respectively. These figures illustrate that the transformation of $\log_{10}(\alpha)$ allows preserving the shape of the original histogram. Additionally, the updated $\log_{10}(\alpha)$ fields without

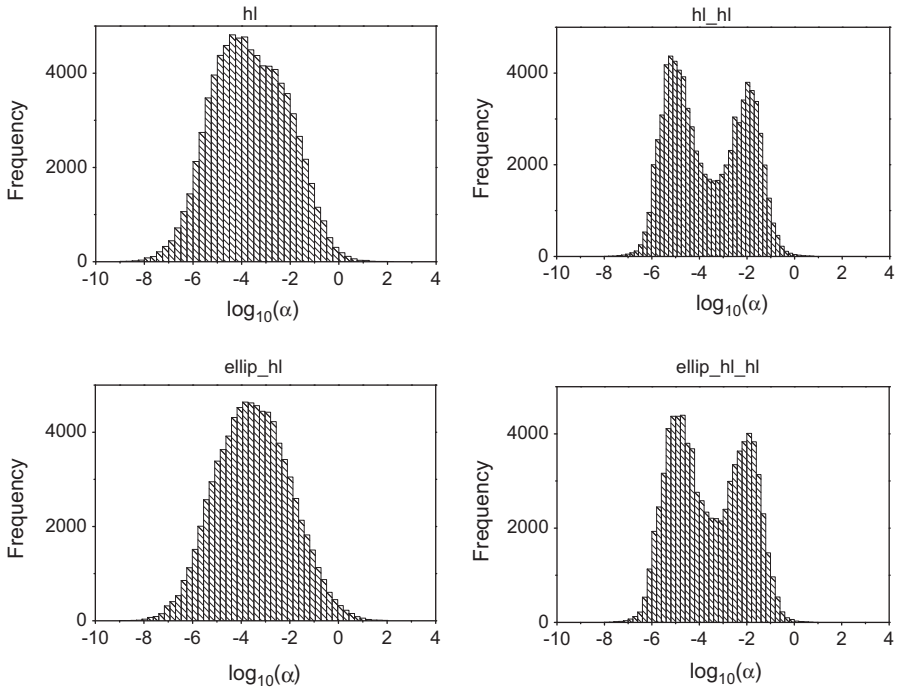

Fig. 12. Histograms of final updated $\log_{10}(\alpha)$ for different scenarios, displayed are values for all river nodes and all stochastic realisations; (upper left) scenario hl: non-MultiGaussian model with channels, updated with EnKF; (upper right) scenario hl_hl: non-MultiGaussian model with channels, updated with NS-EnKF; (bottom left) scenario ellip_hl: non-MultiGaussian model without channels, updated with EnKF; (bottom right) scenario ellip_hl_hl: non-MultiGaussian model without channels, updated with NS-EnKF.

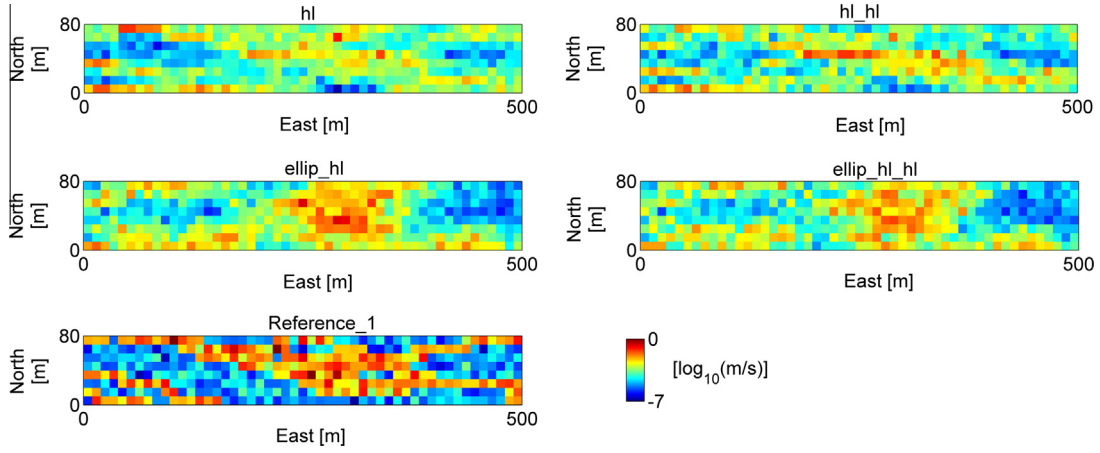

Fig. 13. The reference $\log_{10}(\alpha)$ field together with final updated $\log_{10}(\alpha)$ fields (ensemble mean) for different scenarios: (upper left) scenario hl: non-MultiGaussian model with channels, updated with EnKF; (upper right) scenario hl_hl: non-MultiGaussian model with channels, updated with NS-EnKF; (middle left) scenario ellip_hl: non-MultiGaussian model without channels, updated with EnKF; (middle right) scenario ellip_hl_hl: non-MultiGaussian model without channels, updated with NS-EnKF and (bottom) reference field number 1.

channels (but assuming non-MultiGaussian statistics) represent more realistic riverbed patterns after calibration with NS-EnKF (compared to EnKF). These results indicate that NS-EnKF is able to preserve the initial riverbed hydraulic conductivity patterns. However, these patterns apparently do not yield an improved estimation of the leakage fluxes and leakage coefficients. The boxplots in Fig. 14 show the statistics over ten references which illustrate that both for the non-MultiGaussian model with channels and the non-MultiGaussian model without channels, NS-EnKF is not able to outperform EnKF. There might be multiple reasons for these results. First, leakage coefficients and leakage fluxes can only be improved more than for classical EnKF if the piezometric head data are able to provide more information about $\log_{10}(\alpha)$ than in the standard case. However, the sensitivity of head data for identifying channels is not too high. The results for Section 4.1 already illustrated that the difference between a MultiGaussian and non-MultiGaussian prior model in terms of reproduction of leakage coefficients and leakage fluxes was small. This is illustrative for a limited sensitivity to identify channels. A limitation might be that calculations are very CPU-intensive and therefore limited to 200 stochastic realisations. Especially for NS-EnKF it is important to use a high number of stochastic realisations to determine the anamorphosis function and therefore results for NS-EnKF could be affected by sampling errors induced by the relatively small number of stochastic realisations. However, a test for simulations with 500 realisations gave similar results as for 200 stochastic realisations.

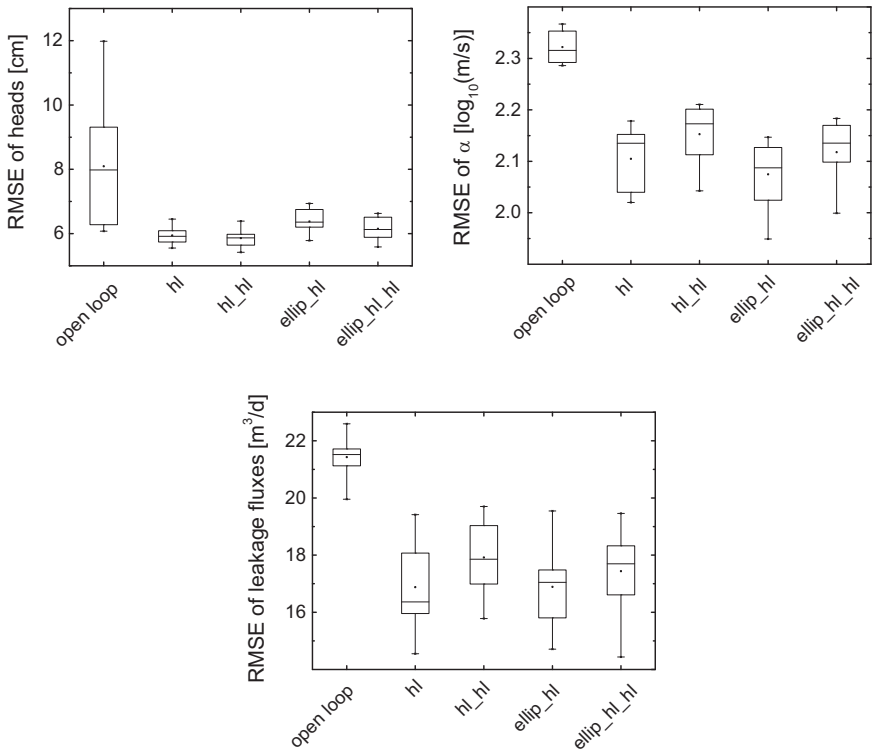

Fig. 14. Boxplot over ten references for (upper left) simulated heads, (upper right) updated $\log_{10}(\alpha)$ and (bottom) estimated leakage fluxes over all model (river) nodes, all realisations and all time steps for different scenarios updated with EnKF (hl and ellip_hl) or NS-EnKF (hl_hl and ellip_hl_hl).

5. Summary and conclusions

This synthetic study investigated for a riverbed displaying non-MultiGaussian structures like channels the impact of the adopted geostatistical model for the inverse characterisation (with Ensemble Kalman Filter (EnKF)) of model states, riverbed properties and river–aquifer exchange fluxes. For aquifers the correct characterisation of channels has an important impact on flow and transport predictions. In this study it is found that the reproduction of channels by multiple-point geostatistical methods results in a better characterisation of states, parameters and fluxes than a MultiGaussian model, but differences are very small compared to a non-MultiGaussian model without channels. This can most probably be explained by the predominant vertical flow through the riverbeds, and the expected horizontal orientation of layers and channels. The conclusion is that non-MultiGaussian riverbed properties have less influence on flow behaviour than non-MultiGaussian hydraulic conductivity distributions in aquifers. We have reached this conclusion using a model that only simulates vertical exchange fluxes between the river and the aquifer. The majority of numerical models (e.g. MODFLOW) are based on a conductance approach, and our analysis suggests that non-MultiGaussian structures do not improve the predictive value of a conductance type model. However, the question has again to be analysed in a 3D, fully coupled model for surface water- groundwater interaction. Such a complimentary study will provide further insight to what extent complexity in the geological structure can improve simulation results for a given model type. It is also expected that heat and solute transport simulations are more sensitive to non-MultiGaussian patterns of riverbed hydraulic conductivities than flow simulations alone. This study tested also whether the Normal-Score Ensemble Kalman Filter was able to give better inversion results than the classical Ensemble Kalman Filter. This could be expected, as hydraulic heads and leakage coefficients did not follow a Gaussian distribution in this study, and Ensemble Kalman Filter performs optimally for Gaussian distributions only, whereas NS-EnKF can handle better bimodal distributions as present in this case. However, the performance of EnKF and NS-EnKF was very similar in this study. This can be related to a too limited sensitivity of piezometric heads to identify channels in the riverbed.

Acknowledgements

The authors gratefully acknowledge the computing time granted on the supercomputer JUROPA at Jülich Supercomputing Centre (JSC). The first author, Qi Tang, also acknowledges the financial support from China Scholarship Council (CSC).

References

Bailey, R., Baù, D., 2010. Ensemble smoother assimilation of hydraulic head and return flow data to estimate hydraulic conductivity distribution. Water Resour. Res. 46 (12).

Bailey, R.T., Baù, D., 2012. Estimating geostatistical parameters and spatially-variable hydraulic conductivity within a catchment system using an ensemble smoother. Hydrol. Earth Syst. Sci. 16 (2), 287–304. http://dx.doi.org/10.5194/hess-16-287-2012.

Bear, J., 1979. Hydraulics of Groundwater. McGraw-Hill, New York, p. 569.

Brunke, M., Gonser, T., 1997. The ecological significance of exchange processes between rivers and groundwater. Freshw. Biol. 37 (1), 1–33. http://dx.doi.org/10.1046/j.1365-2427.1997.00143.x.

Burgers, G., Jan van Leeuwen, P., Evensen, G., 1998. Analysis scheme in the ensemble Kalman filter. Monthly Weather Rev. 126 (6), 1719–1724.

Caers, J., Zhang, T., 2004. Multiple-point geostatistics: a quantitative vehicle for integrating geologic analogs into multiple reservoir models. AAPG Mem. 80, 383–394.

Calver, A., 2001. Riverbed permeabilities: information from pooled data. Ground Water 39 (4), 546–553. http://dx.doi.org/10.1111/j.1745-6584.2001.tb02343.x.

Camporese, M., Paniconi, C., Putti, M., Salandin, P., 2009. Ensemble Kalman filter data assimilation for a process-based catchment scale model of surface and subsurface flow. Water Resour. Res. 45 (10), W10421.

Carrera, J., Alcolea, A., Medina, A., Hidalgo, J., Slooten, L.J., 2005. Inverse problem in hydrogeology. Hydrogeol. J. 13 (1), 206–222.
Carrera, J., Neuman, S.P., 1986. Estimation of aquifer parameters under transient and steady state conditions: 1. Maximum likelihood method incorporating prior information. Water Resour. Res. 22 (2), 199–210.
Chen, Y., Zhang, D., 2006. Data assimilation for transient flow in geologic formations via ensemble Kalman filter. Adv. Water Resour. 29 (8), 1107–1122.
Cheng, C., Song, J.X., Chen, X.H., Wang, D.M., 2011. Statistical distribution of streambed vertical hydraulic conductivity along the Platte River, Nebraska. Water Resour. Manage. 25 (1), 265–285. http://dx.doi.org/10.1007/s11269-010-9698-5.
Crestani, E., Camporese, M., Bau, D., Salandin, P., 2013. Ensemble Kalman filter versus ensemble smoother for assessing hydraulic conductivity via tracer test data assimilation. Hydrol. Earth Syst. Sci. 17 (4), 1517–1531. http://dx.doi.org/10.5194/hess-17-1517-2013.
Delta h Ingenieurgesellschaft mbH, 2006, Spring 3.3, Software, Witten, Germany.
Elfeki, A., Dekking, M., 2001. A Markov chain model for subsurface characterization: theory and applications. Math. Geol. 33 (5), 569–589.
Evensen, G., 1994. Sequential data assimilation with a nonlinear quasi-geostrophic model using Monte Carlo methods to forecast error statistics. J. Geophys. Res.: Oceans (1978–2012) 99 (C5), 10143–10162.
Fleckenstein, J.H., Niswonger, R.G., Fogg, G.E., 2006. River–aquifer interactions, geologic heterogeneity, and low-flow management. Ground Water 44 (6), 837–852. http://dx.doi.org/10.1111/j.1745-6584.2006.00190.x.
Fox, G.A., Durnford, D.S., 2003. Unsaturated hyporheic zone flow in stream/aquifer conjunctive systems. Adv. Water Resour. 26 (9), 989–1000.
Frei, S., Fleckenstein, J.H., Kollet, S.J., Maxwell, R.M., 2009. Patterns and dynamics of river–aquifer exchange with variably-saturated flow using a fully-coupled model. J. Hydrol. 375 (3–4), 383–393. http://dx.doi.org/10.1016/j.jhydrol.2009.06.038.
Gómez-Hernández, J.J., Journel, A.G., 1993. Joint sequential simulation of multiGaussian fields. In: Geostatistics Troia'92. Springer, pp. 85–94.
Gómez-Hernández, J.J., Wen, X.-H., 1998. To be or not to be multi-Gaussian? a reflection on stochastic hydrogeology. Adv. Water Resour. 21 (1), 47–61.
Gómez-Hernánez, J.J., Sahuquillo, A., Capilla, J.E., 1997. Stochastic simulation of transmissivity fields conditional to both transmissivity and piezometric data – 1. Theory. J. Hydrol. 203 (1), 167–174.
Genereux, D.P., Leahy, S., Mitasova, H., Kennedy, C.D., Corbett, D.R., 2008. Spatial and temporal variability of streambed hydraulic conductivity in West Bear Creek, North Carolina, USA. J. Hydrol. 358 (3–4), 332–353. http://dx.doi.org/10.1016/j.jhydrol.2008.06.017.
Guardiano, F.B., Srivastava, R.M., 1993. Multivariate geostatistics: beyond bivariate moments. In: Geostatistics Troia'92. Springer, pp. 133–144.
Hayashi, M., Rosenberry, D.O., 2002. Effects of ground water exchange on the hydrology and ecology of surface water. Ground Water 40 (3), 309–316.
Hendricks Franssen, H.J., Alcolea, A., Riva, M., Bakr, M., Van der Wiel, N., Stauffer, F., Guadagnini, A., 2009. A comparison of seven methods for the inverse modelling of groundwater flow. Application to the characterisation of well catchments. Adv. Water Resour. 32 (6), 851–872.
Hendricks Franssen, H.J., Kaiser, H., Kuhlmann, U., Bauser, G., Stauffer, F., Müller, R., Kinzelbach, W., 2011. Operational real-time modeling with ensemble Kalman filter of variably saturated subsurface flow including stream–aquifer interaction and parameter updating. Water Resour. Res. 47 (2).
Hendricks Franssen, H.J., Kinzelbach, W., 2008. Real-time groundwater flow modeling with the Ensemble Kalman Filter: joint estimation of states and parameters and the filter inbreeding problem. Water Resour. Res. 44 (9).
Hu, L., Chugunova, T., 2008. Multiple-point geostatistics for modeling subsurface heterogeneity: a comprehensive review. Water Resour. Res. 44 (11), W11413.
Irvine, D.J., Brunner, P., Hendricks Franssen, H.J., Simmons, C.T., 2012. Heterogeneous or homogeneous? Implications of simplifying heterogeneous streambeds in models of losing streams. J. Hydrol. 424, 16–23.
Johnson, R.A., Wichern, D.W., 2002. Applied Multivariate Statistical Analysis. Prentice hall Upper Saddle River, NJ, 5.
Kalbus, E., Schmidt, C., Molson, J., Reinstorf, F., Schirmer, M., 2009. Influence of aquifer and streambed heterogeneity on the distribution of groundwater discharge. Hydrol. Earth Syst. Sci. 13 (1), 69–77.
Kerrou, J., Renard, P., Hendricks Franssen, H.J., Lunati, I., 2008. Issues in characterizing heterogeneity and connectivity in non-multiGaussian media. Adv. Water Resour. 31 (1), 147–159.
Khodabakhshi, M., Jafarpour, B., 2013. A Bayesian mixture-modeling approach for flow-conditioned multiple-point statistical facies simulation from uncertain training images. Water Resour. Res. 49 (1), 328–342. http://dx.doi.org/10.1029/2011wr010787.
Kurtz, W., Hendricks Franssen, H.J., Brunner, P., Vereecken, H., 2013. Is high-resolution inverse characterization of heterogeneous river bed hydraulic conductivities needed and possible? Hydrol. Earth Syst. Sci. 17 (10), 3795–3813. http://dx.doi.org/10.5194/hess-17-3795-2013.
Kurtz, W., Hendricks Franssen, H.J., Kaiser, H.P., Vereecken, H., 2014. Joint assimilation of piezometric heads and groundwater temperatures for improved modeling of river–aquifer interactions. Water Resour. Res. 50 (2), 1665–1688. http://dx.doi.org/10.1002/2013wr014823.
Kurtz, W., Hendricks Franssen, H.J., Vereecken, H., 2012. Identification of time-variant river bed properties with the ensemble Kalman filter. Water Resour. Res. 48 (10).
Leek, R., Wu, J.Q., Wang, L., Hanrahan, T.P., Barbet, M.E., Qiu, H.X., 2009. Heterogeneous characteristics of streambed saturated hydraulic conductivity of the Touchet River, south eastern Washington, USA. Hydrol. Process. 23 (8), 1236–1246. http://dx.doi.org/10.1002/hyp.7258.
Li, L., Zhou, H., Hendricks Franssen, H.J., Gómez-Hernández, J.J., 2012. Groundwater flow inverse modeling in non-MultiGaussian media: performance assessment of the normal-score Ensemble Kalman Filter. Hydrol. Earth Syst. Sci. 16 (2), 573–590.
Mariethoz, G., Renard, P., Straubhaar, J., 2010. The Direct Sampling method to perform multiple-point geostatistical simulations. Water Resour. Res. 46 (11).
McCallum, A.M., Andersen, M.S., Rau, G.C., Larsen, J.R., Acworth, R.I., 2014. River–aquifer interactions in a semiarid environment investigated using point and reach measurements. Water Resour. Res. 50 (4), 2815–2829. http://dx.doi.org/10.1002/2012wr012922.
Min, L.L., Yu, J.J., Liu, C.M., Zhu, J.T., Wang, P., 2013. The spatial variability of streambed vertical hydraulic conductivity in an intermittent river, northwestern China. Environ. Earth Sci. 69 (3), 873–883. http://dx.doi.org/10.1007/s12665-012-1973-8.
Pasetto, D., Camporese, M., Putti, M., 2012. Ensemble Kalman filter versus particle filter for a physically-based coupled surface-subsurface model. Adv. Water Resour.
RamaRao, B.S., LaVenue, A.M., De Marsily, G., Marietta, M.G., 1995. Pilot point methodology for automated calibration of an ensemble of conditionally simulated transmissivity fields: 1. Theory and computational experiments. Water Resour. Res. 31 (3), 475–493.
Remy, N., Boucher, A., Wu, J., 2009. Applied Geostatistics with SGeMS: A User's Guide. Cambridge University Press.
Saenger, N., Kitanidis, P.K., Street, R.L., 2005. A numerical study of surface-subsurface exchange processes at a riffle-pool pair in the Lahn River, Germany. Water Resour. Res. 41 (12). http://dx.doi.org/10.1029/2004wr003875.
Salehin, M., Packman, A.I., Paradis, M., 2004. Hyporheic exchange with heterogeneous streambeds: laboratory experiments and modeling. Water Resour. Res. 40 (11), 18. http://dx.doi.org/10.1029/2003wr002567.
Schöniger, A., Nowak, W., Hendricks Franssen, H.J., 2012. Parameter estimation by ensemble Kalman filters with transformed data: approach and application to hydraulic tomography. Water Resour. Res. 48 (4).
Sebok, E., Duque, C., Engesgaard, P., Boegh, E., 2015. Spatial variability in streambed hydraulic conductivity of contrasting stream morphologies: channel bend and straight channel. Hydrol. Process. 29 (3), 458–472. http://dx.doi.org/10.1002/hyp.10170.
Sophocleous, M., 2002. Interactions between groundwater and surface water: the state of the science. Hydrogeol. J. 10 (1), 52–67.
Springer, A.E., Petroutson, W.D., Semmens, B.A., 1999. Spatial and temporal variability of hydraulic conductivity in active reattachment bars of the Colorado River, Grand Canyon. Ground Water 37 (3), 338–344. http://dx.doi.org/10.1111/j.1745-6584.1999.tb01109.x.
Storey, R.G., Howard, K.W.F., Williams, D.D., 2003. Factors controlling riffle-scale hyporheic exchange flows and their seasonal changes in a gaining stream: a three-dimensional groundwater flow model. Water Resour. Res. 39 (2), 17. http://dx.doi.org/10.1029/2002wr001367.
Sun, A.Y., Morris, A.P., Mohanty, S., 2009. Sequential updating of multimodal hydrogeologic parameter fields using localization and clustering techniques. Water Resour. Res. 45 (7).
van Genuchten, M.T., 1980. A closed-form equation for predicting the hydraulic conductivity of unsaturated soils. Soil Sci. Soc. Am. J. 44 (5), 892–898.
Wen, X.-H., Gómez-Hernández, J.J., 1998. Numerical modeling of macrodispersion in heterogeneous media: a comparison of multi-Gaussian and non-multi-Gaussian models. J. Contam. Hydrol. 30 (1), 129–156.
Woessner, W.W., 2000. Stream and fluvial plain ground water interactions: rescaling hydrogeologic thought. Ground Water 38 (3), 423–429. http://dx.doi.org/10.1111/j.1745-6584.2000.tb00228.x.
Wroblicky, G.J., Campana, M.E., Valett, H.M., Dahm, C.N., 1998. Seasonal variation in surface-subsurface water exchange and lateral hyporheic area of two stream–aquifer systems. Water Resour. Res. 34 (3), 317–328. http://dx.doi.org/10.1029/97wr03385.
Zhang, T., 2008. Incorporating geological conceptual models and interpretations into reservoir modeling using multiple-point geostatistics. Earth Sci. Front. 15 (1), 26–35.
Zhou, H., Gómez-Hernández, J.J., Hendricks Franssen, H.J., Li, L., 2011. An approach to handling non-Gaussianity of parameters and state variables in ensemble Kalman filtering. Adv. Water Resour. 34 (7), 844–864.
Zhou, H., Li, L., Hendricks Franssen, H.J., Gómez-Hernández, J.J., 2012. Pattern recognition in a bimodal aquifer using the normal-score ensemble Kalman filter. Math. Geosci. 44 (2), 169–185.
Zinn, B., Harvey, C.F., 2003. When good statistical models of aquifer heterogeneity go bad: a comparison of flow, dispersion, and mass transfer in connected and multivariate Gaussian hydraulic conductivity fields. Water Resour. Res. 39 (3). http://dx.doi.org/10.1029/2001WR001146.